Department of Physics and Astronomy
University of Heidelberg

Bachelor Thesis in Physics
submitted by

Sascha Daniel Diefenbacher

born in Tuttlingen (Germany)

2017

Anomaly Free Vector Mediators

This Bachelor Thesis has been carried out by Sascha Daniel Diefenbacher at the
Institute for Theoretical Physics in Heidelberg
under the supervision of
Prof. Tilman Plehn

Abstract

We extend the Standard Model by a new $U(1)$ gauge symmetry, giving rise to a new Z' gauge boson. Further we introduce an additional scalar S and a dark matter candidate ψ, with the Z' acting as a mediator between the Standard model and the dark sector. The inclusion of the scalar allows the model to be self consistent, since S can gibe mass to the Z', and opens up new search channels. One of these would be $S \to Z'Z$, which would not be possible in a pure Z' model. The main parts of this work consist in producing a consistent model, implementing it into FeynRules and producing Micromegas and Madgraph files with the goal to compute constraints on the model as well as to investigate these novel search channels. We find that the $S \to Z'Z$ search channel can even be a discovery channel improving on previously considered search strategies.

Zusammenfassung

Wir erweitern das Standardmodell mit einer neuen $U(1)$ eich Symmetrie, wodurch ein neues Z' eich boson auftaucht. Zustzlich fhren wir noch einen neuen Skalar S und ein dunkle Materie Kandidaten ψ ein, wobei das Z' as Mediator zwischen dem Standard Modell und dem dunkle Materie Sektor fungiert. Der Skalar sorgt zum einen dafr, dass das Model in sich konsistent ist, da er fr die Masse des Z's verantwortlich sein kann, und ermglicht zum anderen neue Kanle um nach dem Z' zu suchen. Einer dieser Kanle ist $S \to Z'Z$, welcher in einem reinen Z' Modell nicht mglich wre. Der Hauptteil dieser Arbeit besteht daraus ein konsistentes Modell to erstellen, dieses in FeynRules zu implementieren und MadGraph und Micromegas Dateien zu produzieren, mit dem Ziel die Einsuchrnkungen des Modells zu berechnen und die neuen Suchkanle zu untersuchen. Dabei finden wir, dass eine Entdeckung im $S \to Z'Z$ Kanal mglich ist und er eine Verbesserung gegenber zuvor in Betracht gezogenen Suchstrategien darstellt.

Contents

1 Introduction

The Standard Model of particle physics has been very successful in describing the interactions of particles as well as in predicting the results of various experiments. However there are also several questions left unanswered. One of these questions is the nature of dark matter, whose existence is heavily supported through several measurements [1, 2]. Another one is that the gauge group of the Standard Model is a direct product of three symmetry groups: $SU(3)_C$, the strong interaction, $SU(2)_L$, the weak interaction and the hypercharge gauge group $U(1)_Y$. However, there are several other seemingly coincidental global symmetries, and the question can be raised whether the $U(1)_Y$ is the only abelian gauge symmetry.

In this thesis we address both of these questions. By turning one of these global $U(1)$ symmetries into a gauge-group we introduce a new gauge boson Z' that could be the portal to a dark sector. Such Z' models are very popular and have previously been investigated, for example in ref. [3] and [4]. This new boson cannot be massless like the photon, because if it were it would have already been found, since the experimental constraints on massless gauge bosons, even ones with weak couplings, are very strict [5]. Therefore, a mechanism similar to the Higgs mechanism is required to give mass to this new Z'. To this end, we introduce a new scalar field that gives mass to the Z' and that, like the Higgs, has a vacuum expectation value. As a consequence of this the masses of the Z', the scalar and potentially the mass of the dark matter would be proportional to the vacuum expectation value of the new scalar field and a coupling factor. These couplings may not be greater than 4π to ensure the model remains perturbative, and further the coupling of the Z' to the new vev is its gauge coupling, which cannot be too small, in order for collider experiments to be relevant. Therefore, the masses of all the new particles cannot be very different, but rather have to be of the same order of magnitude. This means that there are several new discovery channels involving both the Z' and the scalar that have the potential to not only prove the existence of the Z', but also provide insight into the structure of the dark matter sector.

In order to judge whether these discovery channels are viable and, if they are, in which parameter space, we implement several models with an anomaly free $U(1)$ symmetries in FeynRules. This both allows us to calculate the branching ratios of the new particles and enables us to use a Monte Carlo simulation program, such as MadGraph, to simulate their production cross sections.

2 Anomaly Free Gauge Groups

In order to introduce a new gauge symmetry group and thereby a new conserved charge to the Standard Model, one has to first make sure that the symmetry is not already broken on a quantum level. If this is the case the symmetry is called anomalous. Anomalies may, for example, be caused by loop-level interactions that already violate the charge conservation implied by the symmetry in question [6]. If we want to promote a global symmetry to a gauge symmetry we therefore need to demand that the symmetry is in fact anomaly free. This would mean checking every possible n-loop process for potential anomalies, fortunately we can use the Adler-Bardeen Theorem [7, 8] that states that if a potential anomaly vanishes at one-loop level, it also vanishes at all other loop levels.

The easiest way to check for anomaly cancellation is with fermion triangle diagrams, whereby the contribution of triangle diagrams has to be zero. The contributions are proportional to eq. (1) for the bosons A^a_μ, A^b_ν and A^c_λ, where $t^a ... t^c$ are the generators of the symmetry groups of the respective bosons. Therefore, in order for the individual anomalies to cancel, we only need eq. (1) to be zero [9].

The Standard Model with the $U(1)_Y$, $SU(2)_L$ and $SU(3)_C$ symmetry groups is already anomaly free, as can be seen easily. Since

$$tr[\gamma^5 t^a \{t^b, t^c\}] = 0 \tag{1}$$

the only diagrams that are not zero by definition are shown in fig. 2. For these we can now calculate the contributions:

- $U(1)_Y$ with two $SU(3)_C$

$$tr[t^a t^b Y] = \frac{1}{2}\delta^{ab} Y \sum_q Y_q \tag{2}$$

Here the q in the sum represents a summation over the first generation quark flavors as well as the left- and right handed contributions, with the left handed ones acquiring an additional minus sign. Leptons do not contribute, since the strong interaction does not couple to them:

$$\sum_q Y_q = Y_{u_R} + Y_{d_R} - Y_{u_L} - Y_{d_L} = \Big(\frac{2}{3}\Big) + \Big(-\frac{1}{3}\Big) - 2\Big(\frac{1}{6}\Big) = 0 \tag{3}$$

- $U(1)_Y$ with two $SU(2)_L$

$$tr[\tau^a \tau^b Y] = \frac{1}{2}\delta^{ab} Y \sum_{f_L} Y_{f_L} \tag{4}$$

This time the summation runs over left handed fermion contributions, right-handed ones being left out since they are unaffected by weak interaction. Since both remaining terms a left handed both acquire a minus sign.

$$\sum_{f_L} Y_{f_L} = -3Y_{Q_L} - Y_{E_L} = -3\Big(\frac{1}{6}\Big) - \Big(-\frac{1}{2}\Big) = 0 \tag{5}$$

The factor 3 in the quark charge stems form summing over the 3 color states.

- Three $U(1)_Y$

$$tr[Y^3] = \sum_f Y_f^3 \tag{6}$$

Whereby the sum runs over all fermions charged under U(1)

$$\sum_f Y_f^3 = 3[Y_{u_R}^3 + Y_{d_R}^3 - Y_{u_L}^3 - Y_{d_L}^3] + Y_{e_R}^3 + Y_{\mu_R}^3 - Y_{e_L} \tag{7}$$

$$\sum_f Y_f^3 = 3\left[\Big(\frac{2}{3}\Big)^3 + \Big(-\frac{1}{3}\Big)^3 - 2\Big(\frac{1}{6}\Big)^3\right] - 2\Big(-\frac{1}{2}\Big)^3 + (-1)^3 \tag{8}$$

$$= \Big(\frac{192}{216}\Big) - \Big(\frac{24}{216}\Big) - \Big(\frac{6}{216}\Big) + \Big(\frac{54}{216}\Big) - 1 = 0 \tag{9}$$

- $U(1)_Y$ and 2 gravitons

$$tr[Y] = \sum_f Y_f \tag{10}$$

This does go beyond the Standard Model, since gravity has not yet been quantized, however it seems reasonable to demand that this diagram is also anomaly free.

Again with the sum running over all fermions.

$$\sum_f Y_f = 3[Y_{u_R} + Y_{d_R} - Y_{u_L} - Y_{d_L}] + Y_{e_R} + Y_{\mu_R} - Y_{e_L} \tag{11}$$

$$\sum_f Y_f = 3\left[\Big(\frac{2}{3}\Big) + \Big(-\frac{1}{3}\Big) - 2\Big(\frac{1}{6}\Big)\right] - 2\Big(-\frac{1}{2}\Big) + (-1) = 0 \tag{12}$$

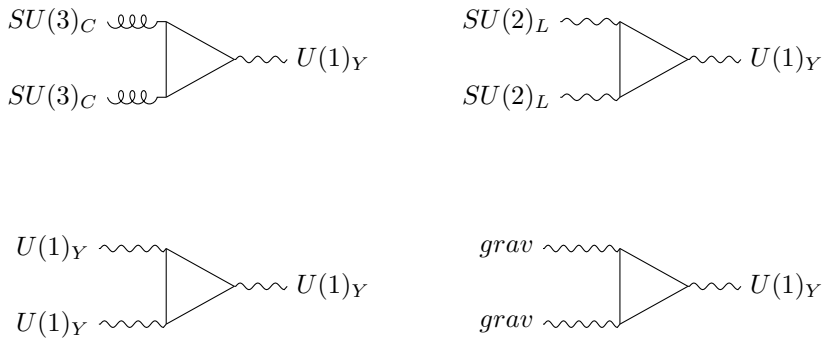

Figure 1: Triangle diagrams contributing to possible gauge anomalies in the SM.

	$SU(3)_C$	$SU(2)_L$	$U(1)_Y$
$\begin{pmatrix} u \\ d \end{pmatrix}_L$	**3**	**2**	$\frac{1}{6}$
u_R	**3**	1	$\frac{2}{3}$
d_R	**3**	1	$-\frac{1}{3}$
$\begin{pmatrix} e \\ \nu \end{pmatrix}_L$	0	**2**	$-\frac{1}{2}$
e_R	0	1	-1

Table 1: Quantum numbers of the SM fermions

As previously stated, the Standard Model with the gauge group $SU(3)_C \times SU(2)_L \times U(1)_Y$ and with the quantum numbers as in table 1 is anomaly free.

When we demand the same from our new symmetry, this greatly limits the possible Standard Model extensions. Introducing a new $U(1)_X$ symmetry (with charges X_i), results in a new table of quantum numbers that can be seen in table 2.

	$SU(3)$	$SU(2)$	$U(1)_Y$	$U(1)_X$
$\begin{pmatrix} u \\ d \end{pmatrix}_L$	**3**	**2**	$\frac{1}{6}$	a
u_R	**3**	1	$\frac{2}{3}$	b
u_R	**3**	1	$-\frac{1}{3}$	c
$\begin{pmatrix} e \\ \nu \end{pmatrix}_L$	0	**2**	$-\frac{1}{2}$	d
e_R	0	1	-1	e

Table 2: Quantum numbers of the SM fermions with a new $U(1)_X$ symmetry.

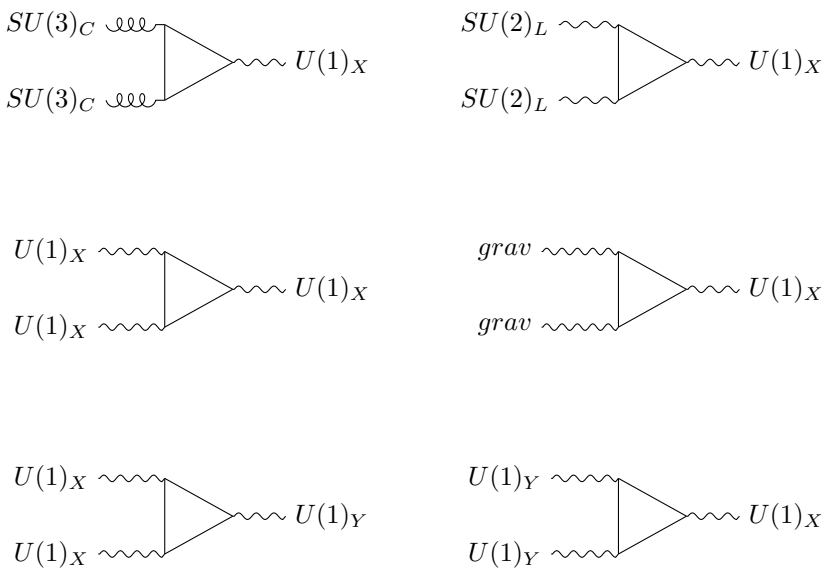

Figure 2: Triangle diagrams contributing to anomalies in the Standard Model with a $U(1)_X$ extension

The new symmetry also results in new anomalous diagrams, seen in fig. (2), that we have to consider.

Just as before the anomalies have to cancel:

- $U(1)_X$ with two $SU(2)_L$:

$$tr[t^a t^b X] = \frac{1}{2}\delta^{ab}\sum_q X_q \tag{13}$$

$$\sum_q X_q = X_{u_R} + X_{d_R} - X_{u_L} - X_{d_L} = 2a - b - c = 0 \tag{14}$$

- $U(1)_X$ with two $SU(2)_L$

$$tr[\tau^a \tau^b X] = \frac{1}{2}\delta^{ab}\sum_{f_L} X_{f_L} \tag{15}$$

$$\sum_{f_L} X_{f_L} = -3X_{Q_L} - X_{E_L} = -3a - d = 0 \tag{16}$$

- Three $U(1)_X$

$$tr[X^3] = \sum_f X_f^3 \tag{17}$$

$$\sum_f X_f^3 = 3(X_{u_R}^3 + X_{d_R}^3 - X_{u_L}^3 - X_{d_L}^3) + X_{e_R}^3 + X_{\nu_L}^3 - X_{e_L}^3 \tag{18}$$

$$= 3(-2a^3 + b^3 + c^3) - 2d^3 + e^3 \tag{19}$$

- $U(1)_X$ and 2 gravitons.

$$tr[X] = \sum_f X_f \tag{20}$$

$$\sum_f X_f = 3(X_{u_R} + X_{d_R} - X_{u_L} - X_{d_L}) + X_{e_R} + X_{\nu_L} - X_{e_L} \tag{21}$$

$$= 3(-2a + b + c) - 2d + e \tag{22}$$

- $U(1)_X$ and two $U(2)_Y$

$$tr[XY^2] = \sum_f X_f Y_f^2 \tag{23}$$

$$\sum_f X_f^2 Y_f = 3[X_{u_R} Y_{u_R}^2 + X_{d_R} Y_{d_R}^2 - X_{u_L} Y_{u_L}^2 - X_{d_L} Y_{d_L}^2] + X_{e_R} Y_{e_R}^2 + X_{\nu_L} Y_{\nu_L}^2 - X_{e_L} Y_{e_L}^2 \tag{24}$$

$$= 3\Big[-2\Big(\frac{1}{6}\Big)^2 a + \Big(\frac{2}{3}\Big)^2 b + \Big(\frac{1}{3}^2\Big)c\Big] - 2\Big(\frac{1}{2}\Big)^2 d + e \tag{25}$$

- Two $U(1)_X$ and one $U(2)_Y$

$$tr[XY^2] = \sum_f Y_f X_f^2 \tag{26}$$

$$\sum_f Y_f X_f^2 = 3[Y_{u_R} X_{u_R}^2 + Y_{d_R} X_{d_R}^2 - Y_{u_L} X 2_{u_L} - X_{d_L} Y_{d_L}^2] + Y_{e_R} X_{e_R}^2 + Y_{\nu_L} X_{\nu_L}^2 - Y_{e_L} X_{e_L}^2 \tag{27}$$

$$= 3\Big[-2\Big(\frac{1}{6}\Big) a^(2) + \Big(\frac{2}{3}\Big) b^2 \Big(\frac{-1}{3}\Big) c^2\Big] - 2(\frac{1}{2}) d^2 + e^2 \tag{28}$$

3 Possible Anomaly Free Extensions

Solving these equations in a general way would be complicated, a simpler and more direct approach consist in taking a symmetry that already exists at tree level and check if it is also anomaly free. This leads to several potential U(1)-symmetries that are anomaly free. Common examples are

1. $U(1)_{B-L}$, meaning the difference between baryon and lepton number is conserved, in this case quarks have a charge of $a = b = c = \frac{1}{3}$ and leptons a universal charge of $d = e = -1$.
2. $U(1)_{L1-L2}$, where L1 and L2 are lepton numbers of different generations, so $e - \mu$, $e - \tau$ or $\mu - \tau$. These models are equivalently anomaly free, however for reasons that will be discussed later $\mu - \tau$ has advantages over the other two. All three models are only anomaly free when the sum over all lepton generations is take into account.

However any difference of a quantum number from one generation and the same number from a different generation can be used as a conserved quantity for a anomaly-free symmetry, as long as eq. (27) is also fulfilled. This can easily be seen as the set of equations is identical for all three fermion generations, therefore taking the difference between two of them always comes out as zero, except for eq.(27) which has quadratic terms.

Therefore $U(1)_{B1-B2}$ would also be a anomaly free group, as would $U(1)_{B2-B3}$, $U(1)_{B1-B3}$ and any possible linear combination of the three, e.g. $U(1)_{B1+B2-2B3}$.

4 Flavor Structures of Anomaly Free Groups

There is also another constraint that needs to be looked at when introducing a new gauge symmetry. The Standard Model Lagrangian contains the expression seen in eq. (29), representing the weak interaction of quarks with the Z boson, the strong interaction, the electromagnetic interaction and the weak interaction with a W boson, in that order.

$$\mathcal{L}_{SM} \supset g_z \overline{Q}_L Z^\mu \gamma_\mu Q_L + g_s \overline{q}_L G^\mu_a \gamma_\mu Q_L T^a_F + g_e \overline{Q}_L A^\mu \gamma_\mu Q_L Q_q + g \overline{u}_L W^+_\mu \gamma^\mu d_L \quad (29)$$

Further, we also have the Yukawa couplings to the Higgs:

$$\mathcal{L}_{SM} \supset \overline{u}_L y_u u_R \frac{1}{\sqrt{2}}(v+h) + \overline{d}_L y_d d_R \frac{1}{\sqrt{2}}(v+h) + h.c. \tag{30}$$

Here u_L and d_L are vectors in flavor space containing the up- and down-type quarks, respectively, and y_d and y_u are 3x3 matrices containing the Yukawa couplings. Now we want to transform the expressions from flavor eigenstates to mass eigenstates, since in collider searches we are only able to observe mass eigenstates of particles. This is done by diagonalizing the Yukawa matrices. In order to do so we insert $V_L^u V_L^{u\dagger} = \mathbb{1}$ and $V_R^u V_R^{u\dagger} = \mathbb{1}$ on either side.

$$\mathcal{L}_{SM} \supset \overline{u}_L V_L^u V_L^{u\dagger} Y_u V_R^u V_R^{u\dagger} u_R \frac{1}{\sqrt{2}}(v+h) + \overline{d}_L V_L^d V_L^{d\dagger} Y_d V_R^d V_R^{d\dagger} d_R \frac{1}{\sqrt{2}}(v+h) + h.c. \tag{31}$$

This allows us to extract:

$$V_L^{u\dagger} Y_u V_R^u = \begin{pmatrix} m_u & 0 & 0 \\ 0 & m_c & 0 \\ 0 & 0 & m_t \end{pmatrix}, \tag{32}$$

$$V_L^{d\dagger} Y_d V_R^d = \begin{pmatrix} m_d & 0 & 0 \\ 0 & m_s & 0 \\ 0 & 0 & m_b \end{pmatrix}. \tag{33}$$

Further we define the new quark mass eigenstate vectors as :

$$\overline{u}'_L = \overline{u}_L V_L^u, \tag{34}$$

$$u'_R = V_R^{u\dagger} u_R, \tag{35}$$

$$\overline{d}'_L = \overline{d}_L V_L^d, \tag{36}$$

$$d'_R = V_R^{d\dagger} d_R. \tag{37}$$

Now we can look at the Standard Model interactions in this new basis and to simplify things we only look at left-handed up-type quarks. Since the only difference between gluon, Z-boson and photon interactions in this case is that gluons and photons couple to left and right handed fermions equally, while the Z-boson couples differently to left-handed and right right-handed ones it is sufficient to look at the term

$$g_z \overline{u}_L Z^\mu \gamma_\mu u_L, \tag{38}$$

to understand the structures.

Since there are no tree-level flavor changing neutral currents in the Standard Model, only left-handed quarks of the same generation couple to one another, so we can write eq. (38) as

$$g_z \overline{u}_L \begin{pmatrix} 1 & 0 & 0 \\ 0 & 1 & 0 \\ 0 & 0 & 1 \end{pmatrix} Z^\mu \gamma_\mu u_L. \tag{39}$$

Once again inserting $V_L^u V_L^{u\dagger} = \mathbb{1}$ and $V_R^u V_R^{u\dagger} = \mathbb{1}$ gives us the expression in the mass eigenbasis.

$$g_z Z^\mu \gamma_\mu \overline{u}_L V_L^u V_L^{u\dagger} \begin{pmatrix} 1 & 0 & 0 \\ 0 & 1 & 0 \\ 0 & 0 & 1 \end{pmatrix} V_L^u V_L^{u\dagger} u_L \tag{40}$$

$$= g_z Z^\mu \gamma_\mu \overline{u}'_L V_L^{u\dagger} \begin{pmatrix} 1 & 0 & 0 \\ 0 & 1 & 0 \\ 0 & 0 & 1 \end{pmatrix} V_L^u u'_L \tag{41}$$

$$= g_z Z^\mu \gamma_\mu \overline{u}'_L V_L^{u\dagger} V_L^u u'_L \tag{42}$$

$$= g_z Z^\mu \gamma_\mu \overline{u}'_L u'_L. \tag{43}$$

This allows us to see that the interaction terms look the same in both mass and flavor eigenbases.

The same can be done for the quark W interactions, for simplicity's sake we will only look at the W^+ case, since it is equivalent to the W^- case,

$$g \overline{u}_L W_\mu^+ \gamma^\mu d_L. \tag{44}$$

Once again, in the interaction base, only quarks of the same generation couple.

$$gW_{\mu}^{+}\gamma^{\mu}\overline{u}_{L}\begin{pmatrix}1&0&0\\0&1&0\\0&0&1\end{pmatrix}d_{L} \tag{45}$$

$$= gW_{\mu}^{+}\gamma^{\mu}\overline{u}_{L}V_{L}^{u\dagger}V_{L}^{u}\begin{pmatrix}1&0&0\\0&1&0\\0&0&1\end{pmatrix}V_{L}^{d\dagger}V_{L}^{d}d_{L} \tag{46}$$

$$= gW_{\mu}^{+}\gamma^{\mu}\overline{u}'_{L}V_{L}^{u}\begin{pmatrix}1&0&0\\0&1&0\\0&0&1\end{pmatrix}V_{L}^{d\dagger}d'_{L} \tag{47}$$

$$= gW_{\mu}^{+}\gamma^{\mu}\overline{u}'_{L}V_{L}^{u}V_{L}^{d\dagger}d'_{L}. \tag{48}$$

The matrix $V_L^u V_L^{d\dagger}$ that couples up-type quarks to down-type quarks is known as the Cabibbo-Kobayashi-Maskawa (CKM) matrix. The entries of the CKM matrix have been measured in experiments with a very high precision, so any new theory has to reproduce it within a very small margin, as can be seen below [10]

$$V_L^u V_L^{d\dagger} = \begin{pmatrix} 0.97472 \pm 0.00015 & 0.22534 \pm 0.00065 & 0.00351^{+0.00015}_{-0.00014} \\ 0.22520 \pm 0.00065 & 0.97344 \pm 0.00016 & 0.0412^{+0.0011}_{-0.0005} \\ 0.00867^{+0.00029}_{-0.00031} & 0.0404^{+0.0011}_{-0.0005} & 0.99146^{+0.000021}_{-0.000046} \end{pmatrix}. \tag{49}$$

Now we can look at what happens when we introduce a new gauge symmetry and therefore a new interaction, for example $U(1)_{B_2-B_3}$, where B_i denotes the baryon family numbers. In this case the term in the Lagrangian has the form:

$$\overline{u}_{L}Z^{\mu}g_{z'}\gamma_{\mu}u_{L}. \tag{50}$$

Consider a flavor non-universal $g_{z'}$:

$$g_{z'} = \begin{pmatrix}0&0&0\\0&1&0\\0&0&-1\end{pmatrix}. \tag{51}$$

In the mass base this becomes

$$\gamma_\mu Z^\mu \overline{u}_L V_L^{u\dagger} V_L^u \begin{pmatrix} 0 & 0 & 0 \\ 0 & 1 & 0 \\ 0 & 0 & -1 \end{pmatrix} V_L^{u\dagger} V_L^u u_L \tag{52}$$

$$= \gamma_\mu Z^\mu \overline{u}'_L V_L^u \begin{pmatrix} 0 & 0 & 0 \\ 0 & 1 & 0 \\ 0 & 0 & -1 \end{pmatrix} V_L^{u\dagger} u'_L. \tag{53}$$

The coupling matrix in the mass base would therefore be

$$V_{Z'} = V_L^u \begin{pmatrix} 0 & 0 & 0 \\ 0 & 1 & 0 \\ 0 & 0 & -1 \end{pmatrix} V_L^{u\dagger}. \tag{54}$$

Now we have no reason to assume that the matrix in eq (54) is diagonal, however since flavor changing neutral currents are experimentally very constrained for a large range of $g_{Z'}$ and $M_{Z'}$ values, this matrix has to be very close to diagonal, otherwise the new model would conflict with reality. Therefore $V_L^{u\dagger}$, V_L^u, $V_L^{d\dagger}$ and V_L^d would have to both diagonalize the matrix in (54) and reproduce the measured CKM matrix. This makes any model that couples different quark generations non-uniformly very unattractive.

This calculation can be performed equivalently for leptons and will give a similar result for models like $L_\mu - L_\tau$, exept instead of reproducing the CKM matrix one would have to reproduce the PMNS (Pontecorvo-Maki-Nakagawa-Sakata) matrix. However, this matrix is far less strictly constrained and the breaking of the symmetry can even explain the structure of the PMNS matrix [11].

The B-L model circumvents this problem completely by having universal quark and lepton couplings, i.e. $g_{z'}$ for quarks is

$$g_{z'q} = \begin{pmatrix} \frac{1}{3} & 0 & 0 \\ 0 & \frac{1}{3} & 0 \\ 0 & 0 & \frac{1}{3} \end{pmatrix}. \tag{55}$$

And for leptons

$$g_{z'L} = \begin{pmatrix} -1 & 0 & 0 \\ 0 & -1 & 0 \\ 0 & 0 & -1 \end{pmatrix}. \tag{56}$$

This causes the total coupling to again be diagonal, similar to eq. (43).

5 Dark Matter

There are several observations which indicate that either our current understanding of gravity is incorrect, or that the universe contains a type of matter that we cannot directly observe. The most prominent of these observations are the results of measuring the rotation curves of galaxies, which do reproduce what would be expected when only visible matter is taken into account. A further indication is the cosmic microwave background (CMB). During the early stages of the universe the temperature dropped low enough for photons to decouple form matter. This allowed those photons to freely propagate through the universe. These photons make up the CMB. Under the assumption that at the time of the decoupling energy was distributed homogeneously throughout the universe, we would expect for the CMB to be homogeneous as well, however this is not the case. One crucial component in explaining these inhomogeneity is the existence of dark matter.

Am important measure for the amount of dark matter in the universe is the so called relic density Ω_Ψ, which is defined as

$$\Omega_\Psi = \frac{\rho_\Psi}{\rho_c}. \tag{57}$$

Where ρ_Ψ is the density of dark matter and ρ_c is the critical density that separates a expanding universe from a collapsing one [12].

Precise measurements of the CMB using the Planck satellite allowed to determine the relic density of dark matter as [13]

$$\Omega_\Psi h^2 = 0.1198 \pm 0.0015. \tag{58}$$

For our model it is vital that we allow for a parameter space in which the relic density that the model predicts is in agreement with the measured one. Since additional dark matter contributions or mediators can modify this calculation, we demand a relic density between 1/3 and 1.1 times the central value.

Phenomenologically the relic density is large when the cross section of dark matter-dark matter annihilation is small and small when the cross section is large. This is rather obvious since a large annihilation cross section reduces the total amount of dark matter and therefore the relic density.

Specifically for our case the dark matter only couples to the Z' and, via the Z-Z' mixing, to the Standard Model Z the only relevant processes are therefore $\overline{\Psi}\Psi \to Z'$ and (to a lesser extent) $\overline{\Psi}\Psi \to Z$. The dark matter to Z' coupling only depends on $g_{Z'}$ and the charge of the dark matter, and can therefore be assumed as constant, so the main factor for the cross section are the masses of the relevant particles. For example if the masses fulfill the relation $M_{Z'} = 2M_{\Psi}$, then the process $\overline{\Psi}\Psi \to Z'$ can happen directly on-shell, leading to the maximal cross section.

6 Three Different Models

For the reasons previously outlined we consider three U(1) extensions to the Standard Model that all lead to a new spin 1 mediator we call Z':

1. $U(1)_X$, here the Z' has no direct coupling to the Standard Model and we use the fact that the Standard Model itself is already anomaly free.
2. $U(1)_{\mu-\tau}$, where the Z' couples to muons, tauons, muon-neutrinos and tauon-neutrinos.
3. $U(1)_{B-L}$, where the Z' couples to all Standard Model fermions.

For all three versions we further introduce a scalar S, which similarly to the Standard Model Higgs boson, breaks the newly introduced symmetry and gives a mass to the Z'.

Finally we also add a dark matter candidate Ψ. The previous discussion about the advantages of anomaly free models would be meaningless if the introduction of Ψ caused an anomaly by itself. In order to ensure that the model remains anomaly free, it is sufficient to make sure that the dark sector is anomaly free, since the Standard Model already has no anomalies under the 3 proposed gauge groups. Since the dark matter candidate only interacts gravitationally and with the Z' we only need to look at eq. (19) and (22). Defining Q_{Ψ_R} and Q_{Ψ_L} as the charge of the right-/left-handed dark matter respectively, this can be written as:

$$0 = Q_{\Psi_R} - Q_{\Psi_L}, \tag{59}$$

$$0 = Q^3_{\Psi_R} - Q^3_{\Psi_L}. \tag{60}$$

Therefore the right- and left-handed components of the dark matter have to have the same charge. This does however mean that the interaction term of dark matter and the new scalar is not gauge invariant.

$$\mathcal{L}_{S\Psi} = \overline{\Psi_L} S \Psi_R. \tag{61}$$

As a consequence of this, there is no dark matter-scalar interaction in the model and the dark matter does not get its mass from the scalar. Instead the nature of the dark matter charges allows us to directly write a mass term, since the expression in eq. (62) is gauge invariant.

$$\mathcal{L} \supset M_\Psi \overline{\Psi} \Psi. \tag{62}$$

This means that, in an anomaly free model, the mass of the dark matter is a completely free parameter that has no connection to the vacuum expectation value of S and by extension to the mass of the Z' or the scalar.

To keep the model as general as possible we introduce kinetic mixing between the new Z' and the Standard Model Z. This leads to a new kinetic term that gets added to the Standard Model Lagrangian:

$$\mathcal{L}_{\text{kin new}} = -\frac{\sin\chi}{2} \hat{Z}'^{\mu\nu} \hat{B}_{\mu\nu} + \frac{1}{4} \hat{Z}'^{\mu\nu} \hat{Z}'_{\mu\nu}, \tag{63}$$

where $\hat{B}_{\mu\nu}$ is the Standard Model hypercharge field strength tensor and χ a parameter describing how large the mixing between Z' and Z is.

Similarly we also allow for mixing between the new scalar and the Higgs boson:

$$\mathcal{L}_{\text{new scalar}} = \frac{1}{2}(D_\mu S)(D^\mu S)^\dagger + \mu_S^2 S^\dagger S + \frac{\lambda'_S}{2}(S^\dagger S)^2 + \lambda_{HS} H^\dagger H S^\dagger S \tag{64}$$

With the covariant derivative $D_\mu = \partial_\mu - i g_{Z'} Q_S Z'_\mu$, the charge of the scalar under the new symmetry Q_S, the gauge coupling of the Z' $g_{Z'}$ and λ_{HS} the mixing parameters for S and the Higgs boson.

In order to implement the Z' couplings described at the beginning of this section, we further introduce the term

$$\mathcal{L}_{Z'} = -g_{Z'} j^\mu_{Z'} Z'_\mu \tag{65}$$

where $j^\mu_{Z'}$ is the current associated with the new symmetry and depends on the version of the model:

$$j^{\mu}_{Z'(X)} = 0, \tag{66}$$

$$j^{\mu}_{Z'(\mu-\tau)} = \overline{\mu}\gamma_{\mu}\mu + \overline{\nu_{\mu}}\gamma_{\mu}\nu_{\mu} - \overline{\tau}\gamma_{\mu}\tau - \overline{\nu_{\tau}}\gamma_{\mu}\nu_{\tau}, \tag{67}$$

$$j^{\mu}_{Z'(B-L)} = \frac{1}{3}\overline{Q}\gamma_{\mu}Q + \frac{1}{3}\overline{u}_R\gamma_{\mu}u_R + \frac{1}{3}\overline{d}_R\gamma_{\mu}d_R + \overline{L}\gamma_{\mu}L + \overline{l}\gamma_{\mu}l. \tag{68}$$

In our model we now have two scalars, the Standard Model Higgs boson, H, and the new scalar, S. Both of them acquire a vacuum expectation value:

$$\langle H \rangle = \frac{v}{\sqrt{2}}, \qquad\qquad \langle S \rangle = \frac{v_S}{\sqrt{2}}. \tag{69}$$

Therefore we can write the fields as:

$$H = \frac{v}{\sqrt{2}} + h, \qquad\qquad S = \frac{v_S}{\sqrt{2}} + s, \tag{70}$$

where s and h are the excitations of the fields. Further, since the potential of the new scalar has to have a minimum at v_S, we get the relation:

$$\frac{v_S^2}{\sqrt{2}} = -\frac{\mu^2}{\lambda'_S}, \tag{71}$$

as well as the terms in the Lagrangian involving the scalars:

$$\mathcal{L} \supset \mu_H^2 H^{\dagger}H + \frac{\lambda'_H}{2}(H^{\dagger}H)^2 + \mu_S^2 S^{\dagger}S + \frac{\lambda'_S}{2}(S^{\dagger}S)^2 + \lambda_{HS}H^{\dagger}HS^{\dagger} \tag{72}$$

Inserting eq. (70) leads to:

$$\begin{aligned}\mathcal{L} \supset\ & \mu_H^2\Big(\frac{v}{\sqrt{2}} + h\Big)^2 + \frac{\lambda'_H}{2}\Big(\frac{v}{\sqrt{2}} + h\Big)^4 + \mu_S^2\Big(\frac{v_S}{\sqrt{2}} + s\Big)^2 \\ & + \frac{\lambda'_S}{2}\Big(\frac{v_S}{\sqrt{2}} + s\Big)^4 + \lambda_{HS}\Big(\frac{v}{\sqrt{2}} + h\Big)^2\Big(\frac{v_S}{\sqrt{2}} + s\Big)^2\end{aligned} \tag{73}$$

$$\begin{aligned}\mathcal{L} \supset & -\lambda'_H \frac{v^2}{\sqrt{2}}\Big(\frac{v}{\sqrt{2}}+h\Big)^2 + \frac{\lambda'_H}{2}\Big(\frac{v}{\sqrt{2}}+h\Big)^4 - \lambda'_S \frac{v_S}{\sqrt{2}}^2\Big(\frac{v_S^2}{\sqrt{2}}+s\Big) \\ & + \frac{\lambda'_S}{2}\Big(\frac{v_S}{\sqrt{2}}+s\Big)^4 + \lambda_{HS}\Big(\frac{v}{\sqrt{2}}+h\Big)^2\Big(\frac{v_S}{\sqrt{2}}+s\Big)^2\end{aligned} \tag{74}$$

Scalar mass terms in the Lagrangian can easily be recognized by their form: $m^2\Psi^\dagger\Psi$. In order to compute the mass mixing matrix we can therefore neglect all terms that do not contain two scalar fields:

$$\begin{aligned}\mathcal{L} \supset & -\lambda'_H \frac{v^2}{2}h^2 + \frac{\lambda'_H}{2}6\frac{v^2}{2}h^2 - \lambda'_S\frac{v_S^2}{2}s^2 + \frac{\lambda'_S}{2}6\frac{v_S^2}{2}s^2 \\ & + \lambda_{HS}\frac{v_S^2}{2}h^2 + \lambda_{HS}\frac{v^2}{2}s^2 + 4\lambda_{HS}\frac{v_S}{2}\frac{v}{2}sh,\end{aligned} \tag{75}$$

$$\begin{aligned}\mathcal{L} \supset & \, 2\lambda'_H\frac{v^2}{2}h^2 + 2\lambda'_S\frac{v_S^2}{2}s^2 \\ & + \lambda_{HS}\frac{v_S^2}{2}h^2 + \lambda_{HS}\frac{v^2}{2}s^2 + 2\lambda_{HS}v_S vsh\end{aligned} \; . \tag{76}$$

This can be expressed in a matrix:

$$\begin{pmatrix} h & s \end{pmatrix}\begin{pmatrix} \lambda'_H v^2 + \frac{\lambda_{HS}}{2}v_S^2 & \lambda_{HS}vv_S \\ \lambda_{HS}vv_S & \lambda'_S v_S^2 + \frac{\lambda_{HS}}{2}v^2 \end{pmatrix}\begin{pmatrix} h \\ s \end{pmatrix} \tag{77}$$

To simplify this we first make the shifts

$$\lambda_H = \lambda'_H + \frac{\lambda_{HS}}{2}\frac{v_S^2}{v^2} \tag{78}$$

$$\lambda_S = \lambda'_S + \frac{\lambda_{HS}}{2}\frac{v^2}{v_S^2} \tag{79}$$

.

With this eq. (77) becomes

$$\begin{pmatrix} h & s \end{pmatrix}\begin{pmatrix} \lambda_H v^2 & \lambda_{HS}vv_S \\ \lambda_{HS}vv_S & \lambda_S v_S^2 \end{pmatrix}\begin{pmatrix} h \\ s \end{pmatrix} \tag{80}$$

.

In order to get the mass eigenbasis we have to diagonalize this matrix. This can be done by multiplying a generic 2 rotation matrix $R(\alpha)$ to both sides.

$$R(\alpha)^\dagger \begin{pmatrix} \lambda_H v^2 & \lambda_{HS} v v_S \\ \lambda_{HS} v v_S & \lambda_S v_S^2 \end{pmatrix} R(\alpha), \tag{81}$$

$$R(\alpha) = \begin{pmatrix} \cos\alpha & \sin\alpha \\ -\sin\alpha & \cos\alpha \end{pmatrix}. \tag{82}$$

This diagonalizes the mass matrix for

$$\tan 2\alpha = \frac{2\lambda_{HS} v v_S}{\lambda_H v^2 - \lambda_S v_s^2}. \tag{83}$$

This transforms the excitations of the scalar fields to:

$$s \to s\cos\alpha + h\sin\alpha, \tag{84}$$

$$h \to h\cos\alpha - s\sin\alpha. \tag{85}$$

Under the assumption that the new scalar is heavier than the Higgs boson this gives the masses of the two particles, which are the diagonal entries of the diagonalized matrix:

$$M_H = \sqrt{\frac{1}{2}(\lambda_H v^2 + \lambda_S v_s^2 - \sqrt{(\lambda_H v^2 - \lambda_S v_s^2)^2 + (2\lambda_{HS} v v_s)^2})}, \tag{86}$$

$$M_S = \sqrt{\frac{1}{2}(\lambda_H v^2 + \lambda_S v_s^2 + \sqrt{(\lambda_H v^2 - \lambda_S v_s^2)^2 + (2\lambda_{HS} v v_s)^2})}. \tag{87}$$

In order to do the same for the Z' we first have to normalize the gauge boson kinetic terms in eq.(63), so we no longer have any mixed terms. To this end we introduce a new basis for the gauge bosons $\hat{B}^\mu, \hat{A}_3^\mu, \hat{Z}'^\mu$, that we can get from the original basis via a non-orthogonal rotation $G(\chi)$:

$$\begin{pmatrix} \hat{B}_\mu \\ \hat{A}_3^\mu \\ \hat{Z}'^\mu \end{pmatrix} = G(\chi) \begin{pmatrix} B_\mu \\ A_\mu^3 \\ Z' \end{pmatrix} = \begin{pmatrix} 1 & 0 & -\tan\chi \\ 0 & 1 & 0 \\ 0 & 0 & \frac{1}{\cos\chi} s \end{pmatrix} \begin{pmatrix} B_\mu \\ A_\mu^3 \\ Z' \end{pmatrix} \tag{88}$$

The Z' itself mixes with the Standard Model gauge bosons B and A^3, leading to a term in the Lagrangian

$$\mathcal{L} \supset \begin{pmatrix} B_\mu & A^3_\mu & Z' \end{pmatrix} \frac{v^2}{4} \begin{pmatrix} g'^2 & -gg' & -g'^2 \tan\chi \\ -gg' & g^2 & gg' \tan\chi \\ -g'^2 \tan\chi & gg' \tan\chi & g'^2 \tan\chi + 2g_{Z'} \frac{v_S^2}{v^2} \frac{\cos\chi^2}{Q_S^2} \end{pmatrix} \begin{pmatrix} B_\mu \\ A^3_\mu \\ Z' \end{pmatrix} \tag{89}$$

The $(1,1)$, $(1,2)$, $(2,1)$ and $(2,2)$ entries of this matrix are consistent with the equivalent 2×2 matrix in the Standard Model. In order to get the expressions for the mass of the Z' and the Z we need to once again diagonalize this matrix. This can again be done by multiplication with two generic rotation matrices $R_1(\xi)$ and $R_2(\Theta_w)$:

$$R_1(\xi) = \begin{pmatrix} 1 & 0 & 0 \\ 0 & \cos\xi & \sin\xi \\ 0 & -\sin\xi & \cos\xi \end{pmatrix}, \tag{90}$$

$$R_2(\Theta_w) = \begin{pmatrix} \cos\Theta_w & \sin\Theta_w & 0 \\ -\sin\Theta_w & \cos\Theta_w & 0 \\ 0 & 0 & 1 \end{pmatrix}. \tag{91}$$

Here ξ is the kinetic mixing angle of the Z' and Θ_w is the Weinberg angle. Appliying the first rotation results in

$$\frac{(g^2+g'^2)v^2}{2} \begin{pmatrix} 0 & 0 & 0 \\ 0 & 1 & t_\chi s_{\Theta_w} \\ 0 & t_\chi s_{\Theta_w} & t_\chi^2 s_{\Theta_w} + \frac{1}{2c_\chi^2} \frac{2g_{Z'}^2 Q_S^2 v_S^2}{(g^2+g'^2)v^2} \end{pmatrix}, \tag{92}$$

with $s_{\Theta_w} = \sin\Theta_w$, $c_\chi = \cos\chi$ and $t_\chi = \tan\chi$.

Substituting $M_Z^2 = \frac{(g^2+g'^2)v^2}{2}$ which is the mass of the Z boson in the Standard Model and $M_{Z\prime}^2 = g_{Z'}^2 Q_S^2 v_S^2$ which is the mass of Z' before the mixing, and diagonalizing the matrix in eq. (92) gives the mass eigenvalues:

$$M_{2,3}^2 = \frac{1}{2}\left[M_Z^2(1 + t_\chi^2 s_\Theta^2) + \frac{1}{2c_\chi^2} M_{Z'}^2 \pm \sqrt{\left(M_Z^2(1 + t_\chi^2 s_\Theta^2) + \frac{1}{2c_\chi^2 M_{Z'}^2} \right)^2 - \frac{2}{c^2} M_{Z'}^2 M_Z^2} \right] \tag{93}$$

The first eigenvalue M_1^2 is zero and corresponds to the photon mass. The second and third eigenvalue are the mass of the Z and Z' which depends on whether we assume the Z-or Z'-mass is higher. From this we can also calculate the kinetic mixing angle

$$\tan 2\xi = \frac{2M_Z^2 t_\chi s_{\Theta_w}}{M_Z^2(1-t_\chi^2)s_{\Theta_w} - \frac{1}{2c_\chi^2}M_{Z'}^2} \tag{94}$$

Now we can define the mass eigenstates of the bosons in relation to their gauge eigenstates:

$$\begin{pmatrix} A^\mu \\ Z_1^\mu \\ Z_2^\mu \end{pmatrix} = R_1(\xi)R_2(\Theta_w)G^{-1}(\chi)R_2^{-1}(\Theta_w) \begin{pmatrix} \hat{A}^\mu \\ \hat{Z}^\mu \\ \hat{Z}'^\mu \end{pmatrix} \tag{95}$$

$$= \begin{pmatrix} 1 & 0 & c_{\Theta_w}s_\chi \\ 0 & c_\xi & c_\chi s_\xi - c_\xi s_\chi s_{\Theta_w} \\ 0 & -s_\xi & c_\chi c_\xi + s_\chi s_{\Theta_w} s_\xi \end{pmatrix} \begin{pmatrix} \hat{A}^\mu \\ \hat{Z}^\mu \\ \hat{Z}'^\mu \end{pmatrix} \tag{96}$$

Or, we can do the inverse using the rotation $K = [R_1(\xi)R_2(\Theta_w)G^{-1}(\chi)R_2^{-1}(\Theta_w)]^{-1}$ with

$$K = \begin{pmatrix} 1 & -c_{\Theta_w}s_\xi t_\chi & -c_{\Theta_w}s_\chi \\ 0 & c_\xi + s_{\Theta_w}s_\xi t_\chi & c_\xi s_{\Theta_w}t_\chi - s_\xi \\ 0 & \frac{s_\xi}{c_\chi} & \frac{c_\xi}{c_\chi} \end{pmatrix}. \tag{97}$$

This finally allows us to write the couplings of the currents to the gauge bosons, as well as the couplings to the scalars

$$\mathcal{L} \supset \begin{pmatrix} ej_{EM} & j_Z \frac{e}{s_{\Theta_w}c-\Theta_w} & j_{Z'}g_{Z'} \end{pmatrix} K \begin{pmatrix} A_\mu \\ Z_\mu \\ Z'_\mu \end{pmatrix} \tag{98}$$

$$\mathcal{L} \supset \begin{pmatrix} A_\mu & Z_\mu & Z'_\mu \end{pmatrix} K^\dagger \begin{pmatrix} 0 & 0 & 0 \\ 0 & \frac{M_Z^2}{2v}(v + c_\alpha h - s_\alpha s) & 0 \\ 0 & 0 & \frac{M_{Z'}^2}{2v_S}(v + c_\alpha s + s_\alpha h) \end{pmatrix} K \begin{pmatrix} A_\mu \\ Z_\mu \\ Z'_\mu \end{pmatrix} \tag{99}$$

7 Details of the Implementation

To simplify the later simulations we had to decide on a set of free parameters to scan over. For these we chose $M_{Z'}$, M_S, λ_{HS} to determine the strength of the Higgs-S mixing and χ for the $Z - Z'$ mixing. In addition to this we keep both Q_S and $g_{Z'}$ constant. This allows us to calculate the remaining parameters. Further we will from here on refer to the new scalar as S.

$$\lambda_S = \frac{M_S^2 + M_H^2 + \sqrt{(M_S^2 - M_H^2)^2 - (2\lambda_{HS} v v_S)^2}}{(2v_S^2)}, \tag{100}$$

$$\lambda_H = \frac{(M_S^2 + M_H^2)}{v^2} - \frac{\lambda_S v_S^2}{v^2}, \tag{101}$$

$$v_S = \frac{\sqrt{2}\cos\chi M_{Z'}\sqrt{M_{Z'}^2 - M_Z^2 - M_Z^2 s_{\Theta_w}^2 \tan\chi^2}}{g'\sqrt{M_{Z'}^2 - M_Z^2} Q_S}. \tag{102}$$

We note that the vev of S, v_S, is already fixed by only $M_{Z'}$ and χ. Further, we use the Standard Model masses of the Z boson and the Higgs boson for M_Z and M_H and the Standard Model Higgs vev for v. This allows us to ensure that the model remains consistent with the current measurements of the Standard Model.

The models itself was implemented using the Mathematica [14] package FeynRules [15, 16], which allows for automated Feynman rules calculation. We also used FeynRules to directly calculate the analytical expressions for the decay widths of both Z' and S into individual channels that were later used to determine the branching ratios.

8 Implementation of the Relic Density Constraint

For the calculation of the relic density the program Micromegas [17] was used. Micromegas is based on the CalcHEP [18] package, using it to calculate the tree level cross sections relevant for interactions of the dark matter candidate, that then in turn can be used to calculate the relic density. The implementation of the model itself has been performed by taking advantage of the FeynRules CH output.

We used this setup to scan over a varying range of parameters. The first plot (fig. (3)) shows the relic density for different Z' and dark matter masses. The area between the red lines indicates the parameter-spaces where the relic density has the desired value. In the plot we can see two valleys of low relic density, one at $M_\Psi \approx$ 45 GeV, which is about half the mass of the Standard Model Z boson, and one along

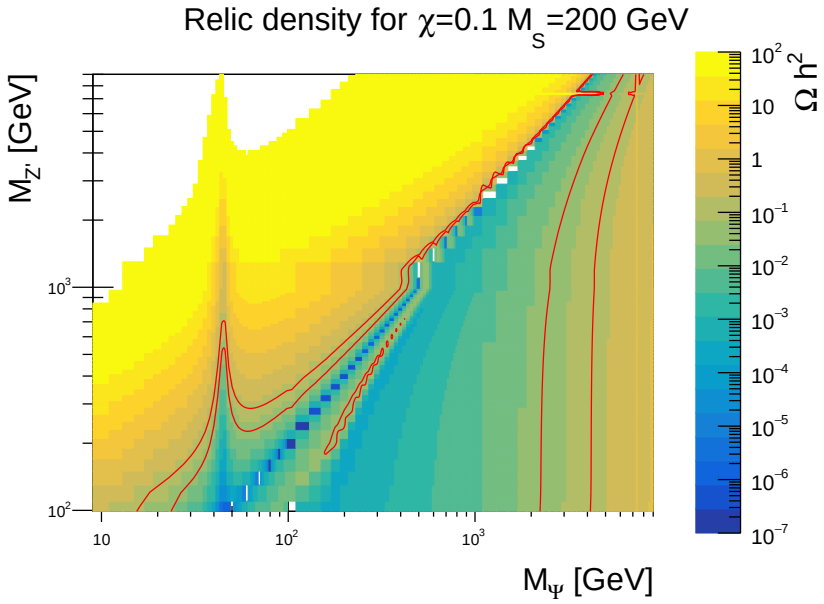

Figure 3: Relic density plot for different Z' and dark matter masses, sections between the red lines have the desired relic density

the area where $M_\Psi \approx \frac{M_{Z'}}{2}$. This is exactly as expected, since the annihilation cross sections are the highest if either of the on-shell conditions is met. For values of M_ψ slightly higher than $\frac{M_{Z'}}{2}$ the relic density drops of again. In order determine the reason for this, we can use the fact that Micromegas can not only compute the relic density, but also records which processes were the most relevant for a specific pair of parameters. From this we see that at the drop off happens when $2M_\Psi \approx M_S + M_{Z'}$. This is relevant since the scan was performed using the model in which the Z' has no couplings to the Standard Model outside of the mixing with the Z. This means the only tree level couplings of the Z' are with the scalar. Therefore the process $\overline{\Psi} + \Psi \to Z'^* \to Z' + S$ is relevant when compared to $\overline{\Psi} + \Psi \to Z' \to X_{SM} + X_{SM}$, despite requiring an off-shell Z' propagator.

Lastly, we can see that there are several areas where our model produces the right relic density, the one left of the $M_\Psi \approx \frac{M_{Z'}}{2}$ valley is the most relevant for our searches, since this allows for decays of Z' into dark matter, enabling a potential Z' to invisible collider search.

In fig. (4) we can see the effect of the kinetic mixing parameter χ has on the relic density. For convenience the corresponding values of ξ were also printed along the y-axis. We note, however, that ξ and χ do not have a linear relation to each other. Once again we can make out three valleys, one at $M_\Psi = \frac{M_Z}{2}$, one at $M_\Psi = \frac{M_{Z'}}{2}$ and a last one at $M_\Psi = \frac{M_{Z'}+M_S}{2}$, corresponding to the three annihilation channels mentioned above. To explain the structures, we need to look at how the individual

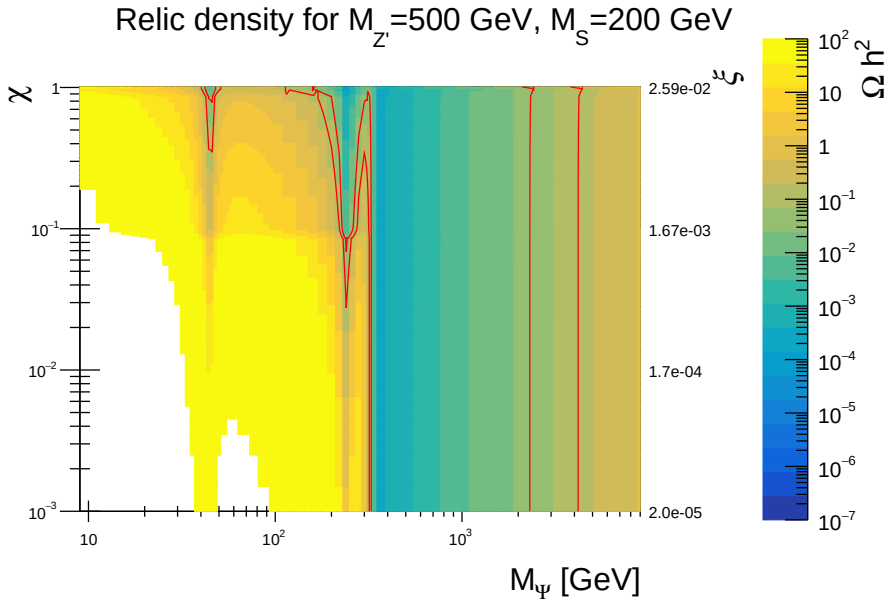

Figure 4: Relic density plot for and dark matter masses and mixing parameters χ, sections between the red lines have the desired relic density

channels depend on the χ, in relation to each other.

1. $\overline{\Psi}+\Psi \to Z \to X_{SM}+X_{SM}$. The first vertex is proportional to $\left(\frac{s_\xi}{c_\chi}\right)^2$ as we will see later the c_χ^2 in the denominator appears in all channels, so we will neglect it. The second vertex is proportional to $\left(c_\xi + s_{\Theta_w} s_\xi t_\chi - c_{\Theta_w} s_\xi t_\chi\right)^2$, since ξ is so small we can drop the terms containing s_ξ, resulting in $(c_\chi)^2$. This annihilation channels is therefore approximately proportional to $s_\xi^2 c_\chi^2$

2. $\overline{\Psi} + \Psi \to Z' \to X_{SM} + X_{SM}$. The first vertex is proportional to $\left(\frac{c_\xi}{c_\chi}\right)^2$, and once again we can ignore the denominator. The second vertex is proportional to $\left(c_\xi s_{\Theta_w} t_\chi - s_\xi - c_{\Theta_w} s_\chi\right)^2$. Again we can assume that $c_\xi \approx 1$ and $s_\xi \approx 0$ giving us: $\left(s_{\Theta_w} t_\chi - c_{\Theta_w} s_\chi\right)^2$ which behaves proportional to s_χ, as long as χ is not too big. Of course the second coupling of the vertex does not seem be relevant here, since it describes a decay, which will always eventually happen, no matter how small the coupling. After all the Z' is not stable. However, we have to keep in mind that while the dark matter mass is below the $\frac{M_{Z'}}{2}$ threshold a decay of Z' is also possible and since dark matter to dark matter processes are not relevant for the relic density we do have to take the second vertex's coupling into account. For this explanation the approximation that the channel is proportional to $s_\chi^2 c_\xi^2$ is sufficient.

3. $\overline{\Psi} + \Psi \to Z'^* \to S + Z'$. Like in the previous channel the first vertex is

proportional to $\left(\frac{c_\xi}{c_\chi}\right)^2$. The second vertex is proportional to $\left(\frac{c_\xi^2}{c_\chi^2}\right)^2$. Once again assuming $c_\xi \approx 1$, the channel is proportional to $\frac{1}{c_\chi^4}$.

This means that both channels that have Standard Model final states have larger cross sections when χ, and therefore ξ, is larger, in an approximately linear relation. In the plot this can be seen as the relic density along the first two valleys getting smaller, and the valley getting wider. Meanwhile, the third valley attributed to the SZ' final state barely changes depending on the mixing angles. The only effect can be seen in the region where χ approaches 1.

9 Branching Ratios

9.1 Z' Branching Ratios

In order to judge what channels could prove useful in the search for our Z' we first look at the branching ratios of the Z' as well as the scalar for different Masses and mixing angles.

The Z' has the following decay channels:

1. Tree level: Depending on which model is used, Z' either has tree level couplings only to dark matter, dark matter and two lepton generations ($L_1 - L_2$) or to dark matter as well as all fermions of the Standard Model ($B - L$). These channels will be dominant once kinematically allowed, however if the dark matter is heavy enough and the Z' has no Standard Model tree level couplings, there might be mass region where the Z' can only decay via the mixing.
2. Z-Z'-Mixing: Since the Z' mixes with the Z boson it can decay into the same final states as the Z boson. This also allows the Z' to radiate a S and then mix into a Z, leading to a ZS final state. Further the Z' also gains a coupling to the EM current through the mixing, as can be seen in eq. (98) and (97). This gives the $Z\prime$ additional photon-like couplings. Therefore the branching ratios of the Z' are different than those of the Z. However these channels are all suppressed by the mixing angle and therefore only really relevant as long as no tree level decays are possible.

For each of the models we will now look at the branching ratios of the Z' individually.

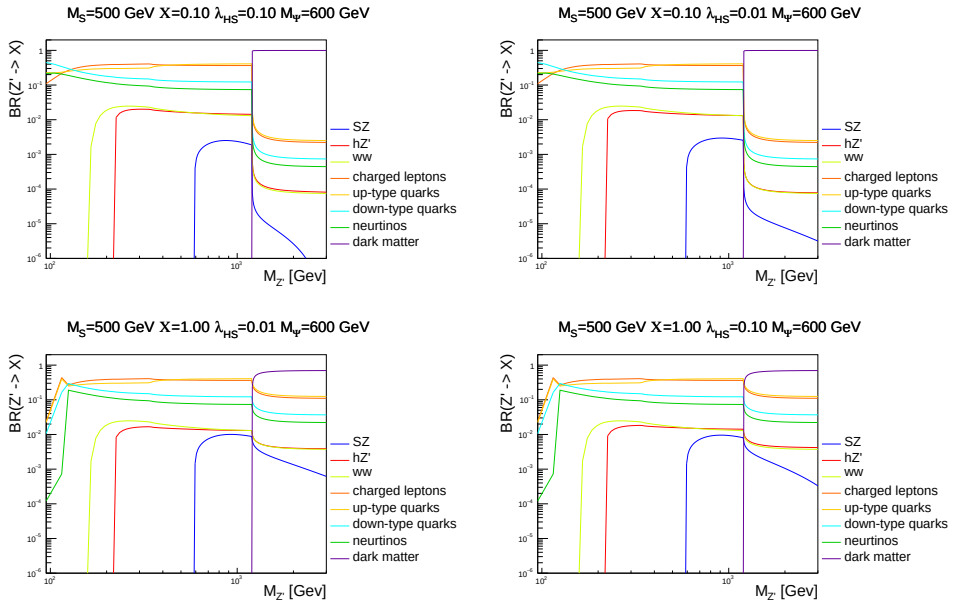

Figure 5: Branching ratios Br($Z' \to$ X) for M_S=500 GeV, $g_{Z'} = 1$, M_ψ =600 GeV and different values of χ and λ_{HS}, $U(1)_X$ model

9.1.1 $U(1)_X$

Fig. (5) shows the branching ratios of the Z' in a model where the non-mixing Z' coupling is to dark matter. As expected the dark matter decay channel is dominant, as soon as $M_{Z'} \geq 2M_\psi$. Even for a large mixing of $\chi = 1$ it exceeds the other channels by at least an order of magnitude.

In the fermion channels several effects can be observed, for one there is a 50% increase in the up-type branching ratio at around 350 GeV, that corresponds to the $\bar{t}t$ channel opening up. Further the charged lepton channel starts out with a low branching ratio, only to then supersede the other fermion channels. This is caused by the fact that the coupling of the Z' to the EM- current j_{EM} only scales with χ, while the coupling to the neutral current scales with both χ and ξ (see ep. (98) and (97)). However, for a constant χ, ξ gets smaller as the difference between M_Z and $M_{z'}$ increases (eq. 94). Therefore, the couplings of the Z' are closer to those of the Z for low masses and closer to those of a photon for large masses, and since the coupling of the Z to charged leptons is weaker than that of the photon, the charged lepton branching ration increases for larger Z' masses.

Finally we can see that the decay into SZ exists and scales with the scalar-Higgs-mixing parameter λ_{HS}, but it is way to small to be helpful in collider searches. A search in the lepton channels, especially muons, would be a lot more promising.

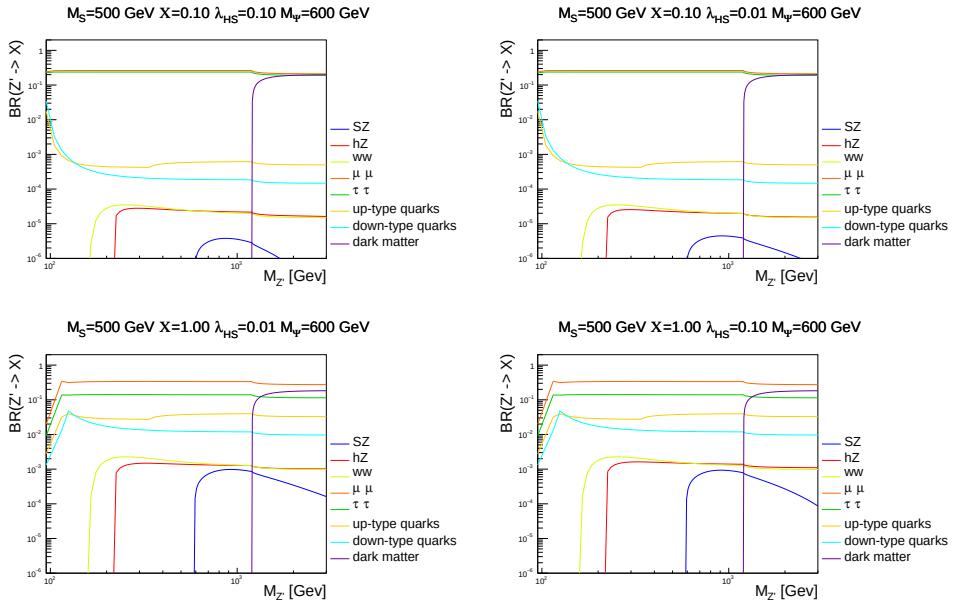

Figure 6: Branching ratios Br($Z' \to$ X) for M_S=500 GeV, $g_{Z'} = 1$, M_ψ=600 GeV and different values of χ and λ_{HS}, $U(1)_{\mu-\tau}$ model

9.1.2 $U(1)_{\mu-\tau}$

For low values of χ the branching ratios is fig. (6) behave just as expected, muon-, tauon (and their respective neutrino-, left out in the plot for readability) decays are dominant, until the dark matter decay becomes possible, from then on the muon, tauon and dark matter decays are equally likely. It is no surprise that the SZ contribution is even smaller in this scenario. For models like this a search in lepton channels wins out by far.

There is, however, another interesting effect to be seen. Once we increase χ the muon and tauon channels no longer have the same branching ration. To better observe this we plot plot the muon, tauon and neutrino branching ratios in relation to χ in fig. (7).

In this we can see that the branching ratio of muons and muon neutrinos increases for higher values of χ, while the tauon and tauon neutrino ratios decrease. This is caused by the fact that under the new symmetries muons and muon neutrinos have a charge of $+1$ and tauons and tauon neutrinos have a charge of -1. In the Lagrangian the terms that describe the coupling of the Z' to these leptons can be written like this.

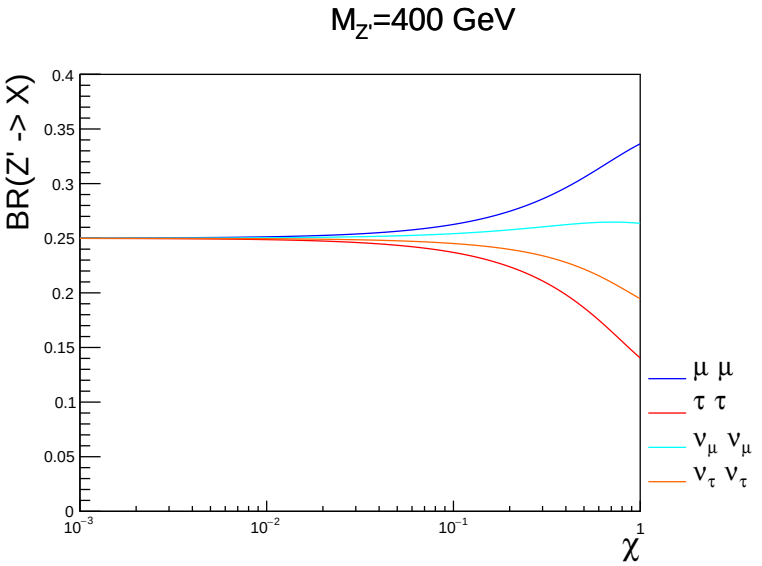

Figure 7: Branching ratios Br($Z' \to$ X) for $M_{Z'} = 400$ GeV depending on the mixing parameter χ

$$\begin{aligned}\mathcal{L} \supset & Z'^{\mu}\overline{\mu}\gamma_{\mu}\mu(Q_{\mu}k_{Z'} + k_{\text{mix}}) \\ & + Z'^{\mu}\overline{\nu_{\mu}}\gamma_{\mu}\nu_{\mu}(Q_{\mu}k_{Z'} + k_{\text{mix neutr}}) \\ & + Z'^{\mu}\overline{\tau}\gamma_{\mu}\tau(Q_{\tau}k_{Z'} + k_{\text{mix}}) \\ & + Z'^{\mu}\overline{\nu_{\tau}}\gamma_{\mu}\nu_{\tau}(Q_{\tau}k_{Z'} + k_{\text{mix neutr}})\end{aligned} \tag{103}$$

Where Q_{μ} and Q_{τ} are the $U(1)_{\mu-\tau}$ charges of muons and tauons, $k_{Z'}$ describes the contribution to the vertices coming from the tree level Z' interaction and k_{mix} and $k_{\text{mix neutr}}$ are the contribution from the Z-Z' mixing, which is smaller for neutrinos, since the neutrino contribution only comes from the interaction with j_Z while the one for charged leptons originates form both the interactions with jZ and j_{EM}. These factors contribute quadratic in the matrix elements, that are therefore proportional to:

$$((1)k_{Z'} + k_{\text{mix}})^2, \tag{104}$$

$$((-1)k_{Z'} + k_{\text{mix}})^2. \tag{105}$$

This shows that a larger mixing contribution actually decreases the coupling

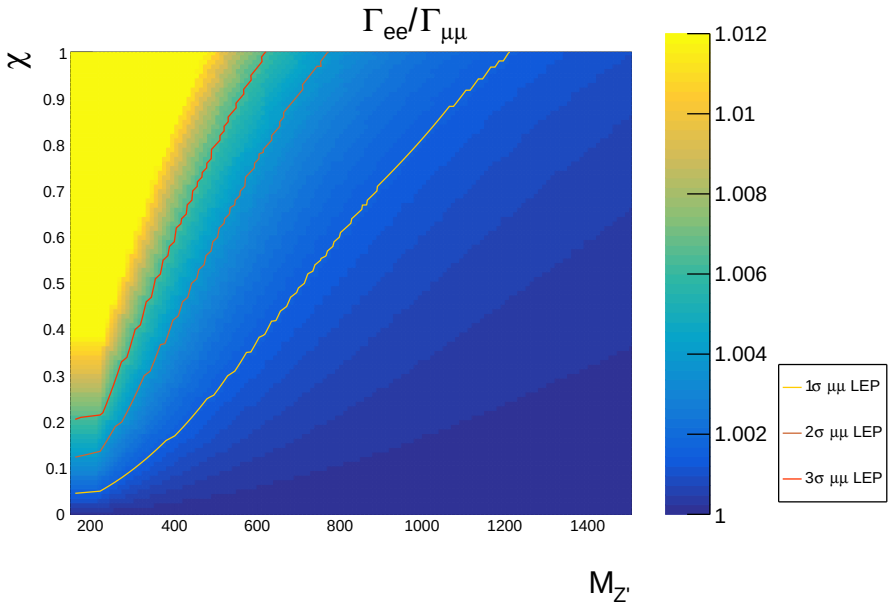

Figure 8: Simulated ratio between decay widths of $(Z' \to e^+e^-)$ and $(Z' \to \mu^+\mu^-)$ for different mixing parameters and Z' masses.

of the Z' to the lepton generation with a negative charge under the new interaction.

9.1.3 $U(1)_{\mu-\tau}$ LEP Constraints

Similar to how the Z-Z' mixing has an effect on the Z' branching ratios, it also has effects on the branching ratios of the Standard Model Z. This is was not the case in the previous model, since the Z' has to have direct couplings to the Standard Model for this effect to occur. These ratios have been however measured very precisely at the Large Electron Positron Collider (LEP) as [10]

$$\frac{\Gamma_{ee}}{\Gamma_{tot}} = (3.363 \pm 0.004)\%,$$

$$\frac{\Gamma_{\mu\mu}}{\Gamma_{tot}} = (3.366 \pm 0.007)\%.$$

From this we can calculate the ratio between the two:

$$\frac{\Gamma_{ee}}{\Gamma_{\mu\mu}} = 0.9991 \pm 0.0024 \tag{106}$$

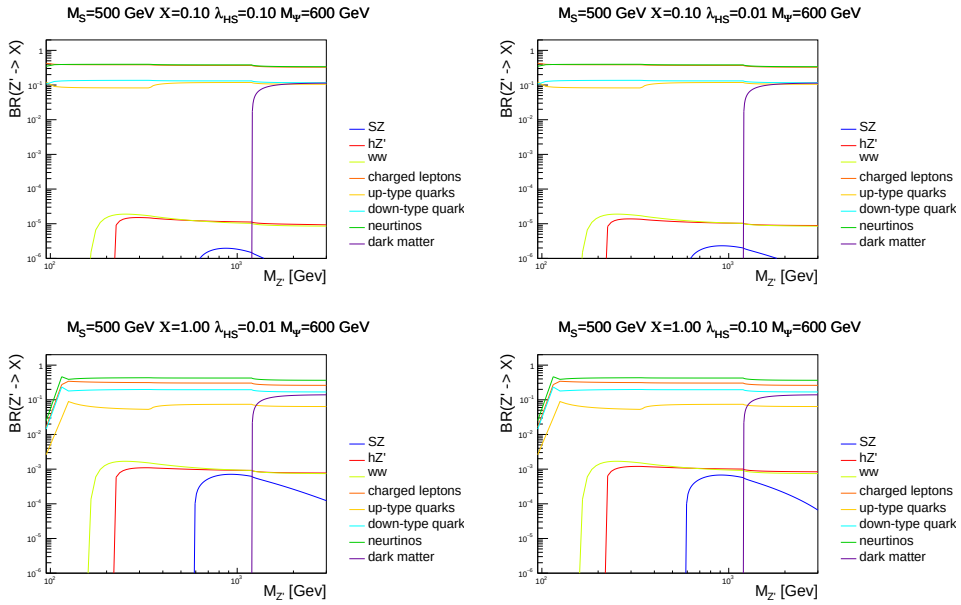

Figure 9: Branching ratios Br($Z' \to$ X) for M_S=500 GeV, $g_{Z'} = 1$, M_ψ=600 GeV and different values of χ and λ_{HS}, $U(1)_{B-L}$ model.

This ratio can also be calculated in the $U(1)_{\mu-\tau}$ model. This was done in fig. (8). Here we see the ratio from eq. (106) plotted as heat-map in for different Z' masses and values of χ. Further there are three lines drawn representing the points where the simulated ratio is one, two or three sigma different from the measured one.

From this we see that especially for heavier Z' masses the mixing is barely constrained.

9.1.4 $U(1)_{B-L}$

In this model the Z' has tree level couplings to all fermions. Therefore the decays into fermions are the dominant ones, as can be seem in fig. (9). The model behaves very similarly to the previously discussed $U(1)_{\mu-\tau}$ model, in that for large χ the mixing has an effect on the branching ratios, causing the ratios for up- and down-type quarks and charged and uncharged leptons to no longer be the same. Furthermore the ZS channel is even more suppressed than before.

9.2 S Branching Ratios

There are three ways for the new scalar S to decay:

1. In an absence of mixing the only tree level interaction of S is with Z'. Since all other couplings are inadvertently suppressed relative to this, the $Z'Z'$ decay channel will be dominant once it is kinematically allowed.

2. Via the mixing with the Higgs. Since S and H mix it is possible for the S to mix into a Higgs and then decay into the same final states that the Standard Model Higgs can decay into, namely WW, ZZ and $\bar{t}t$. These channels are suppressed relative to the mixing angle α, however as long as the above mentioned $Z'Z'$ channel is not allowed this does not matter, because S is not stable and has to decay. The mixing with the Higgs also leads to a SHH vertex, that allows for a decay into two Higgs bosons.

3. Via the Z-Z' mixing. It is possible for S to decay into two Z's, and then have one of the Z's mix into a Standard Model Z. This is possible once the scalar mass is larger than the combined mass of Z' and Z. The likelihood if this process is largely dictated by the Z-Z' mixing. This mixing also allows for the case where both Z's mix into Zs, resulting in a ZZ final state, however this is twice suppressed by the mixing angle.

The results of the branching ratio calculation are plotted in fig. (10). As predicted if both the Z-Z'-mixing and scalar-mixing are set to zero the scalar only decays into two Z', once M_S is greater than $2M_{Z'}$. Allowing Z-Z'-mixing, the ZZ as well as the ZZ' channel open up, once they are kinematically allowed, while the scalar mixing allows S to decay through the same channels as the Standard Model Higgs could decay. If both mixings are allowed the two sets of channels compete against each other, and as would be expected a large scalar-mixing and small Z-Z'-mixing means the Higgs channels are dominant, and vice versa for small scalar- and large Z-Z'-mixing.

Also shown in the branching ratio plot are several regions where the parameters are excluded by other constraints. The first one is that λ_S has to stay below 4π in order for the theory to remain perturbative. This is only relevant for large masses of S. Furthermore, the Higgs mixing is also constrained by experimental results [19], which is why parameter spaces with $\sin\alpha > 0.4$ are excluded. The mass restriction stems form the fact that for a given λ_{HS} the mass of S and the mass of the Higgs cannot be to close to each other. This is because, as can be seen from eq. (87) and eq. (86), there is a minimal difference between M_H and M_S that scales with λ_{HS}, vs and v. In the plot itself this can be seen as a small slice of the parameter space around the mass of the Higgs that is forbidden since the scalar mass and the Higgs mass would be to close.

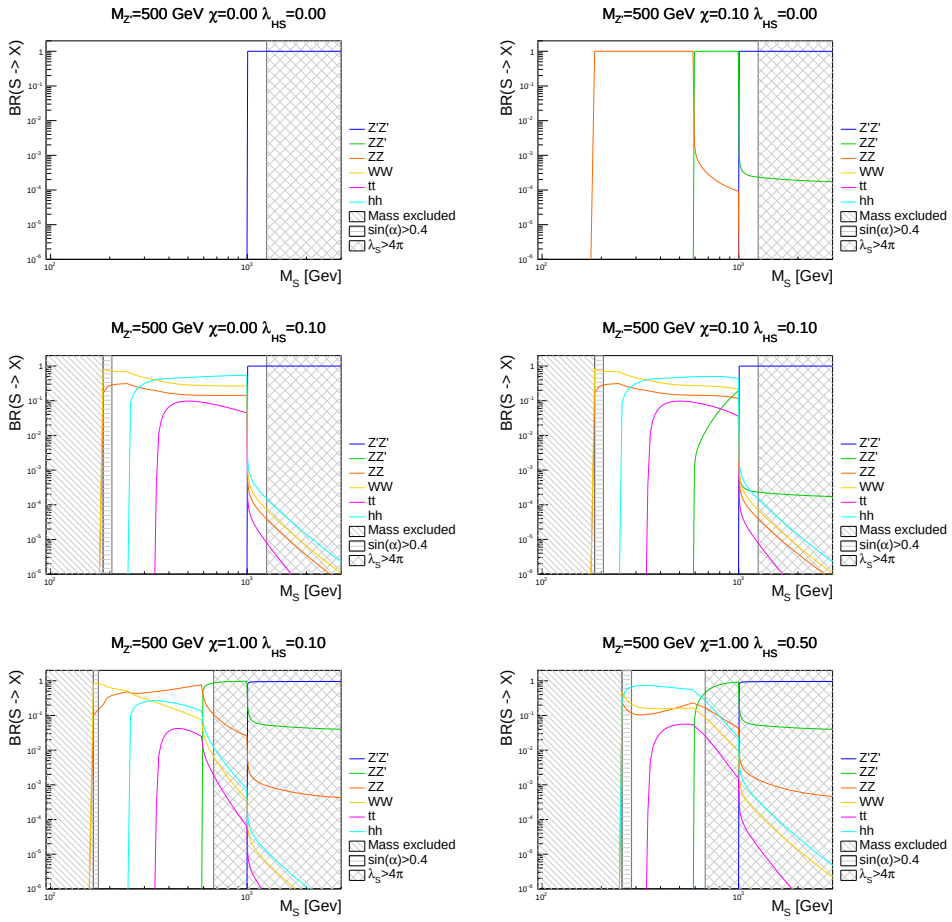

Figure 10: Branching ratios Br($Z' \to$ X) for M_S=500 GeV, $g_{Z'} = 1$, M_ψ=600 GeV and different values of χ and λ_{HS}.

We can see that a parameter space exists where a search in the $S \to Z' + Z$ channel would be worthwhile. However to actually decide this we also need to look at the total cross section of the $p + p \to S \to Z' + Z$ process. For this we need to determine the production cross section of S and then multiply it with the branching ratios.

10 S Production Cross Section

The only way of producing the new scalar in a collider is via the mixing with the Higgs boson, therefore the production channels of S are the same as for the Higgs in the Standard Model. The most important ones of those is gluon-gluon fusion, and vector boson fusion for large masses of S. The Feynman diagram for this can be seen in fig. (10). An economic way to implement this interaction would be to add an effective ggS vertex. In order to obtain this effective vertex one would have to integrate out the top quark in the loop, however this only makes sense if the mass of the top is larger than the mass of the new scalar. Since we do not want to constrain ourselves to these relatively small mass scales the only other way is to simulate the loop process. In practice this means creating a NLO (Next-to-Leading Order) model file to run in a Monte Carlo simulation program such as MadGraph [20]. FeynRules itself comes with a package named NLOCT [21], that allows the calculation of NLO counter terms, further the extension FeynArts [22] is capable of generating the needed NLO diagrams. FeynRules already has a functioning FeynArts interface.

The first step consists of renormalizing the Lagrangian. FeynRules can do this automatically and is able to output the result in the appropriate FeynArts format. This can be rather time consuming, mostly depending on the size of the Lagrangian that has to be renormalized as well as the number of internal parameters in the model, e.g. using only external parameters that have a predefined value makes this a matter of minutes, while trying to renormalize the model with the full set of dependent parameters as described above can take several hours on a single laptop CPU. Another thing to keep in mind is that the existence of tadpoles in the model causes problems when writing the output for FeynArts. Unfortunately the terms in eq. (64) introduces such tadpoles, once the scalar fields assume a vev, therefore we drop all terms that are not relevant to our searches, in other words only terms with the order HHS and HS are used.

Next we can use this FeynArts file to generate the NLO diagrams and calculate the counter terms. Here we can also impose restrictions, such as only taking QCD processes into account or neglecting terms involving 4 scalars. The end result is a .nlo file containing the new vertices induced by loop diagrams.

Finally we can use this .nlo file in conjunction with the original FeynRules

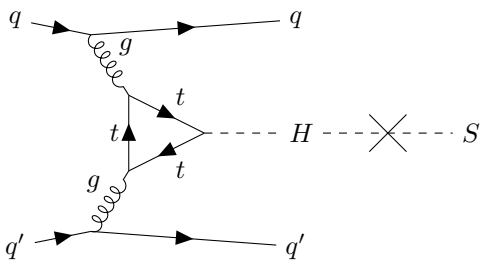

Figure 11: Production of the new scalar via gluon gluon fusion

model to generate a UFO (Unified FeynRules Output) model file. It is of note0 that the last steep seems to cause problems when using Mathematica on iOS, while both Windows and Linux based systems function just fine.

We can use this model to simulate events in MadGraph, simply by loading the file and running MadGraph in NLO-mode. This is done by adding [QCD] after the to be generate process. For example to test the generation of the scalar through gluon-gluon-fusion one runs:

```
generate p p > s0 [QCD]
```

The [QCD] indicates which interaction orders should contribute to the considered loop diagrams, since for the purpose of simulating gluon gluon fusion QCD is the only relevant interaction.

In order to verify the simulation we plot the result, the Higgs gluon-gluon fusion cross section taken from the LHC Working Group [23], the same Higgs cross section multiplied by $\sin\alpha^2$ in the same plot and the cross section of Higgs gluon-gluon fusion simulated with the Standard Model NLO model provided by MadGraph. This is show in fig. (12).

We can see that the curve that represents our simulation has the correct shape. There is a significant difference between our simulated cross section and the one that we would expect based on the Higgs production cross section given in [23]. This same difference is already present in the comparison between the leading order Higgs production cross section produced with MadGraph and the LHC working group prediction. This is the case because for our simulation we only looked at $gg \to H$, at one-loop level. The results form the LHC Working Group on the other hand include both higher order processes, as well as processes like $gg \to H + jet$.

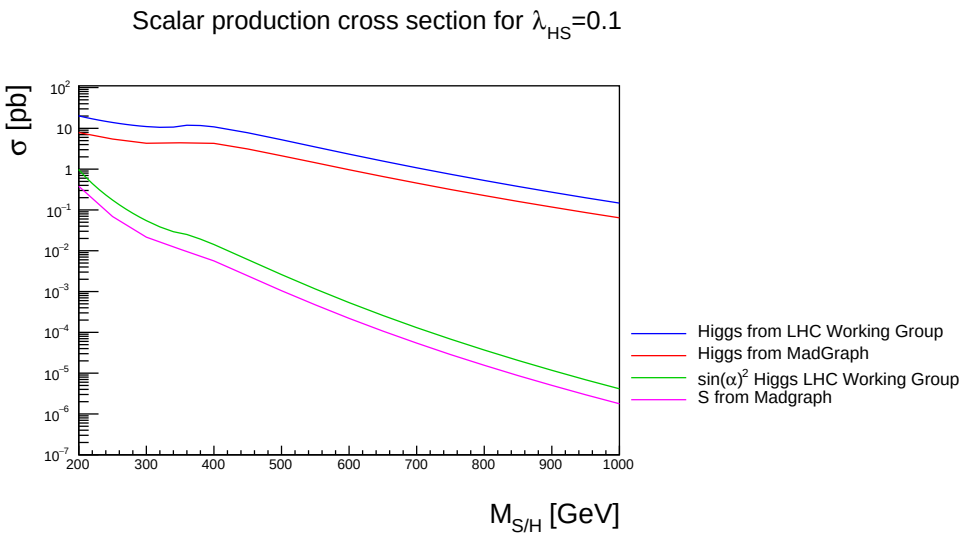

Figure 12: Production cross section of the Higgs and S at different masses for $\lambda_{HS} = 0.1$ and $\sqrt{s}$=14 TeV

10.1 Total $pp \to S \to Z'Z$ Cross Section

Using the branching ratios and the production cross section of S from the previous sections we can now calculate the total cross section for the channel of interest. We decided to use the Higgs cross sections from [23] and scale them by $\sin(\alpha)^2$ for this calculation, since otherwise we would have to run a new simulation for every relevant value of the scalar mixing. This also allows us to include contributions for other production channels such as vector-boson fusion, which could be relevant at high scalar masses.

Fig. (13) shows the product of the production cross section and the branching ratios, as well as the same exclusion areas that were used in the plots of the S branching ratio. We did this for several combinations of λ_{HS} and χ, as well es for two different Z' masses. The first thing to notice is that for a Z' with a mass of 500 GeV the cross section of $pp \to S \to Z'Z$ is to low to be detectable at the LHC. This is because, as we can see from ref. [24] we would require about 30-40 events for a discovery in in a resonant mono-Z search. For an integrated luminosity of 100fb^{-1} and a $Z \to ee/\mu\mu$ of about 7% [10] this means the cross section would have to be at least 5fb to be deletable. For a lighter Z' there is, however, a parameter space where the channel would be viable. In this parameter space λ_{HS} cannot be to large, otherwise the decays via the mixing with the Higgs would be dominant, but λ_{HS} also dictates the production cross section of S, meaning it also cannot be to low. Similarly, a sufficiently large χ is needed to ensure the decay into $Z'Z$ happens often enough, however a large χ and a simultaneously small $M_{Z'}$ requires a comparatively small vev of S, as can be seen in eq.(102). This means that for large χ scalar masses big enough

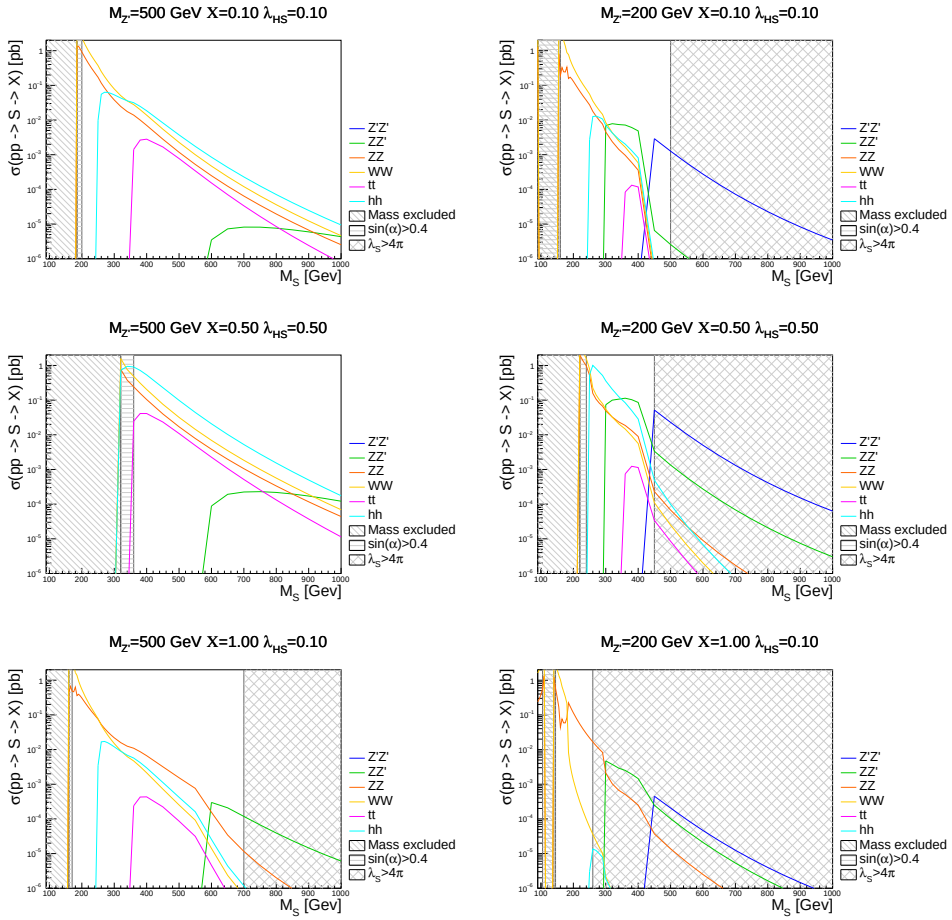

Figure 13: Total cross sections for $pp \to S \to Z'Z$ for $M_{Z'}$=200 GeV and $M_{Z'}$=500 GeV, $\sqrt{s}$=14 TeV and different values of χ and λ_{HS}.

to allow for $S \to Z'Z$ are excluded, as can be seen in the lowest plot on the right in fig. (13).

11 Searches

There are three different strategies to measure couplings of a Z' from an anomaly free gauge group to dark matter.

11.1 Mono Jet

Mono jet searches are the standard approach for dark matter searches at colliders. The process, where a Z' gets produced via the Z-Z' mixing and then decays into dark matter is invisible for the detector. However, if a jet is produced along the way, it results in a visible signal, usually with a high amount of missing energy and missing transversal momentum caused by the invisible dark matter. Unfortunately a simple decay of the Z' into neutrinos would result in a similar signature. Therefore, one would have to see a excess in Z' to invisible events compared to what the model without Z'-dark matter couplings predicts. In these searches the background for signals with low amounts of missing energy is rather large. In order to isolate the Z'-dark matter couplings they need to be differentiated from model-dependent $Z' \to \nu\bar{\nu}$ decays. This requires precision measurements in the mono-jet channel, which are challenging due to the large backgrounds. The precision does increase for higher missing energy values, meaning a mono jet search would be most effective when we predict the Z' to be heavy.

11.2 $S \to Z'Z$

As seen in the previous section, there is a parameter space for which the channel $pp \to S \to Z'Z$ is viable. This allows us to search for a mono-Z signature, which is significantly more precise than a jet search. Furthermore, this channel would not only indicate the existence of a Z', but also give further insights into the structure of the dark sector, since the $Z'Z$ channel is only possible if the model also includes S. From fig. (13) we know that this channel only works for a lower mass Z'. Since resonant mono-Z production is considerably cleaner than the mono-jet search, it is a promising search to determine Z'-dark matter couplings in the presence of other missing energy signatures such as $Z' \to \nu\bar{\nu}$.

11.3 $Z' \to l^+ l^-$

A third strategy consists in measuring the width of the Z if it is discovered in dilepton final states. This is especially promising for $U(1)_{\mu-\tau}$ and $U(1)_{B-L}$ models, since here the Z' has direct couplings to the leptons, however as seen in fig(5) this search can even be viable for $U(1)_X$ models when the Z'-Z mixing is large enough. A fit to the total width of the mediator can then reveal the presence of a dark matter final state.

12 Conclusion and Outlook

In this thesis we try to correlate two pressing questions left unanswered by the SM: Is there a portal to dark matter, and is one of the anomaly free global symmetries gauged?

We have introduced a new gauge boson to the Standard Model as a potential dark matter mediator. Beyond that we also introduced a new scalar, giving mass to the new gauge boson and thereby making the model self consistent and opening up search-channels not present in models without the scalar. We investigated whether such a model is able to reproduce the measured dark matter relic density and analyzed potential the search-channels for collider experiments that could allow us to discover the existence of our model.

In doing so, we found that there is a large parameter space in which the model reproduces the desired relic density. This shows that the mass of the Z' is not constrained by the relic density.

Further, we discovered that the partial width of the $Z' \to SZ$ decay channel is too small for it to be a relevant search channel. However a parameter space exists where the process $S \to ZZ'$ is both the dominant channel for S decays and has a large enough total cross section to produce a potential discovery signal.

This channel not only has the potential to discover such a mediator, but further can isolate the coupling of the Z' to dark matter. In this function, this search is complementary and extends the reach of mono-jet searches, for which precision measurements to isolate $Z' \to DM$ from $Z' \to \nu\bar{\nu}$ decays is challenging. In order to find out whether this channel is as promising as it seems it has to be compared to other potential searches. To this end we will simulate the production and decay of S, and run an analysis on the resulting data that searches for a mono-Z (in the form of a lepton pair) plus missing energy signal. Performing the same simulation and analysis for the most important background processes will allow us to estimate the signal/background ratio of this channel.

Further, we will investigate whether the Z', after decaying into Standard Model

particles via the Z-Z' mixing could be seen as a mass peak in measurements. Because the width of this peak will depend on the couplings of the Z', we can then attempt to fit a function to this mass peak that will give insight into the nature of the Z'. For example one could see if the Z' has couplings to dark matter.

Finally, we will run a mono-jet simulation and analysis as a benchmark for the other two searches.

Using these results will allow us to precisely determine what search is the most promising for different sets of parameters.

Acknowledgments

I would, fist of all, like to thank Prof. Dr. Tilman Plehn both for giving me the chance to work in his research group on such an interesting topic and for being there to discuss physics problems.

Further I would like to say thank you to Dr. Martin Bauer, for taking the time to answer the many question I had throughout working with him, as well as for proof reading this thesis.

In the same vein my sincerest gratitude to Daniel Camargo for his advice on FeynRules and Micromegas as well as the new physics of the model.

And finally i want to thank the entire LHC Physics and New Particles research group, not only for their frequent help with questions, but also for making me feel welcome.

References

[1] D. Clowe, A. Gonzalez and M. Markevitch, Astrophys. J. Weak lensing mass reconstruction of the interacting cluster 1E0657-558: Direct evidence for the existence of dark matter, arXiv:astro-ph/0312273.

[2] Wayne Hu, Scott Dodelson, Cosmic Microwave Background Anisotropies, arXiv:astro-ph/0110414.

[3] Julian Heeck and Werner Rodejohann, Gauged $L_\mu - L_\tau$ symmetry at the electroweak scale, *Phys. Rev. 84, 075007*, 2011, doi:10.1103/PhysRevD.84.075007.

[4] Xiao-Gang He, G. C. Joshi, H. Lew, and R. R. Volkas, Simplest Z model, *Phys. Rev. 44, 2118*, 1991, doi:10.1103/PhysRevD.44.2118.

[5] J.L. Hewett et al., Fundamental Physics at the Intensity Frontier, arXiv:1205.2671 [hep-ex].

[6] Matthew D. Schwartz, *Quantum Field Theory and the Standard Model*, Cambridge University Press, 2014.

[7] S. Adler, Axial-Vector Vertex in Spinor Electrodynamics, *Phys. Rev. 177, 2426*, 1969.

[8] Bell, J.S., Jackiw, R. Nuovo Cimento A (1965-1970) (1969) 60: 47. https://doi.org/10.1007/BF02823296.

[9] Daniel V. Schroeder and Michael Peskin, *An Introduction To Quantum Field Theory*, Addison-Wesley Advanced Book Program, 1995.

[10] J. Beringer et al. (Particle Data Group), PR D86, 010001 (2012), http://pdg.lbl.gov.

[11] J. Heeck and W. Rodejohann, *Phys. Rev. 85, 113017*, 2012 doi:10.1103/PhysRevD.85.113017 [arXiv:1203.3117 [hep-ph]].

[12] Tilman Plehn, Yet Another Introduction to Dark Matter, arXiv:1705.01987 [hep-ph].

[13] Planck Collaboration, Planck 2015 results. XI. CMB power spectra, likelihoods, and robustness of parameters, arXiv:1507.02704 [astro-ph.CO].

[14] Wolfram Research, Inc., Mathematica, Version 11.2, Champaign, IL (2017).

[15] Adam Alloul, Neil D. Christensen, Celine Degrande, Claude Duhr, Benjamin Fuks, FeynRules 2.0 - A complete toolbox for tree-level phenomenology, arXiv:1310.1921 [hep-ph].

[16] Neil D. Christensen, Claude Duhr, FeynRules - Feynman rules made easy, arXiv:0806.4194 [hep-ph].

[17] G. Belanger, F. Boudjema, A. Pukhov and A. Semenov, arXiv:1305.0237 [hep-ph].

[18] Alexander Belyaev, Neil D. Christensen, Alexander Pukhov, CalcHEP 3.4 for collider physics within and beyond the Standard Model, arXiv:1207.6082 [hep-ph].

[19] Guillaume Chalons, David Lopez-Val, Tania Robens, Tim Stefaniak, The Higgs singlet extension at LHC Run 2, arXiv:1611.03007 [hep-ph].

[20] J. Alwall, R. Frederix, S. Frixione, V. Hirschi, F. Maltoni, O. Mattelaer, H.-S. Shao, T. Stelzer, P. Torrielli, M. Zaro, The automated computation of tree-level and next-to-leading order differential cross sections, and their matching to parton shower simulations, arXiv:1405.0301 [hep-ph].

[21] C. Degrande, Automatic evaluation of UV and R2 terms for beyond the Standard Model Lagrangians: A proof-of-principle, Comput.Phys.Commun. 197 (2015) 239-262.

[22] T. Hahn, Generating Feynman Diagrams and Amplitudes with FeynArts 3, arXiv:hep-ph/0012260.

[23] LHC Higgs Cross Section Working Group, Handbook of LHC Higgs Cross Sections: 1. Inclusive Observables, arXiv:1101.0593 [hep-ph].

[24] The ATLAS collaboration, Search for high-mass resonances decaying into a Z boson pair in the final state in pp collisions at $sqrts$=13 TeV with the ATLAS detector, ATLAS-CONF-2016-012, 2016.

Erklärung

Ich versichere, dass ich diese Arbeit selbstständig verfasst und keine anderen als die angegebenen Quellen und Hilfsmittel benutzt habe.

Heidelberg, den 16.10.2017

Sascha Daniel Diefenbacher